

RESEARCH PAPER



Molecular modelling insights into a physiologically favourable approach to eicosanoid biosynthesis inhibition through novel thieno[2,3-*b*]pyridine derivatives

Mosaad S. Mohamed^a, Yara E. Mansour^a, Hatem K. Amin^b and Moustafa E. El-Araby^{a*}

^aDepartment of Pharmaceutical Organic Chemistry, Faculty of Pharmacy, Helwan University, Cairo, Egypt; ^bDepartment of Biochemistry and Molecular Biology, Faculty of Pharmacy, Helwan University, Cairo, Egypt

ABSTRACT

In this research, we exploited derivatives of thieno[2,3-*b*]pyridine as dual inhibitors of the key enzymes in eicosanoid biosynthesis, cyclooxygenase (COX, subtypes 1 and 2) and 5-lipoxygenase (5-LOX). Testing these compounds in a rat paw oedema model revealed potency higher than ibuprofen. The most active compounds **7a**, **7b**, **8b**, and **8c** were screened against COX-1/2 and 5-LOX enzymes. Compound **7a** was the most powerful inhibitor of 5-LOX with $IC_{50} = 0.15 \mu M$, while its *p*-chloro analogue **7b** was more active against COX-2 ($IC_{50} = 7.5 \mu M$). The less desirable target COX-1 was inhibited more potently by **8c** with $IC_{50} = 7.7 \mu M$. Surflex docking programme predicted that the more stable *anti*- conformer of compound (**7a**) formed a favourable complex with the active site of 5-LOX but not COX-1. This is in contrast to the binding mode of **8c**, which resembles the *syn*-conformer of series **7** and binds favourably to COX-1.

ARTICLE HISTORY

Received 12 February 2018
Revised 16 March 2018
Accepted 21 March 2018

KEYWORDS

Anti-inflammatory; COX-2;
5-LOX; COX-1;
thieno[2,3-*b*]pyridine



Introduction

Eicosanoids are arachidonic acid (AA) metabolites that comprise prostaglandins (PGs) and leukotrienes (LTs), the principal inflammatory mediators in osteoarthritis (OA)^{1,2}. PGs and LTs play key roles in triggering the failure of innate homeostasis of chondrocytes that contribute to pain, swelling, joint damage, and other symptoms of OA^{3,4}. PGs' biosynthesis starts when cyclooxygenases (COXs) catalyse two reactions, first the bis-peroxidation of AA to PGG₂ and second, the reduction of the acyclic peroxide group in PGG₂ to form the key precursor PGH₂. PGH₂ metabolises, according to elicited biological needs, to responsive PGs under catalysis of various prostaglandin synthases⁵.


The "mostly" inducible subtype cyclooxygenase-2 (COX-2) is greatly upregulated during the inflammatory processes while the constitutive subtype COX-1 is "mostly" assigned to the regulation of PGs in healthy individuals³. In 1990s, the approach of selective inhibition of COX-2 by coxibs was sought as the imminent strategy to control OA, taking the advantage of less side effects than the classic non-steroidal anti-inflammatory drugs (NSAIDs, Figure 1)⁶. NSAIDs (non-selective inhibitors of COX 1&2), though widely used as analgesics and anti-inflammatory drugs to date, are frequently implicated in a variety of adverse actions. Patients under NSAIDs frequently report GI inflammation, bleeding, ulcers, in addition to hepatic problems, renal toxicities, and others². However, only few years after the first coxib approval, rofecoxib, and valdecoxib (Figure 1) were withdrawn from world markets subsequent to findings of links to increased cardiovascular events such as atherosclerosis and infarction^{7,8}. Other coxibs and some NSAIDs had to add warnings to their labels and limitation of uses in certain patients with risks of cardiovascular complications⁹.

Before withdrawals, some valuable studies placed selective COX-2 inhibitors under scrutiny as evidences accumulated about COX-1 and COX-2 overlapping functions. COX-1's role was proved not to be limited to "housekeeping" as it was widely claimed in literature¹⁰. COX-1 was found to contribute considerably to some inflammatory responses¹¹ leading to decreased efficacy of some COX-2 selective inhibitors unless they exert a minimum of COX-1 inhibition at the therapeutic dose¹². Moreover, COX-2 is constitutively expressed in certain tissues to catalyse the biosynthesis of some beneficial PGs such as PGI₂, a critically needed prostaglandin for homeostasis of the cardiovascular system¹³. Therefore, the clinical use of COX1/2 inhibitors will remain associated with some undesirable effects regardless being a selective coxib or a non-selective NSAID¹⁴. Moreover, shutting down the COX1/2 pathway causes a shunting of AA to the other proinflammatory route, the lipoxygenase (LOX) pathway. This possibly results in decreased efficacy¹⁵ as well as aggravation of GI side effect of NSAIDs¹⁶. Encoding gene of 5-lipoxygenase (5-LOX), the key enzyme for biosynthesis of the inflammatory mediators LTs, is almost undetectable in healthy individual¹⁷ but activated during various inflammatory events¹⁸. Inhibitors of 5-LOX (e.g. Zileuton, Figure 1) are compassionately prescribed for controlling some inflammatory disorders such as bronchial asthma¹⁹, but it is much less efficacious in OA²⁰ regardless the proven involvement of 5-LOX in arthritic progression^{21,22}.

Based on undisputable findings, dual inhibitors for both COX1/2 and 5-LOX pathways should provide superior efficacies in controlling inflammation and pain in patients suffering from OA with less adverse effects²³. For instance, dual COX1/2–5LOX inhibitors demonstrated excellent analgesic and anti-inflammatory activities with lower gastric irritation, bleeding and ulcerogenic side effects.

CONTACT Moustafa E. El-Araby  madaoud@kau.edu.sa  Department of Pharmaceutical Organic Chemistry, Faculty of Pharmacy, Helwan University, Cairo 11790, Egypt

*Current address: Department of Pharmaceutical Chemistry, Faculty of Pharmacy, King Abdulaziz University, Jeddah, Saudi Arabia.

 Supplemental data for this article can be accessed [here](#).

© 2018 The Author(s). Published by Informa UK Limited, trading as Taylor & Francis Group.

This is an Open Access article distributed under the terms of the Creative Commons Attribution License (<http://creativecommons.org/licenses/by/4.0/>), which permits unrestricted use, distribution, and reproduction in any medium, provided the original work is properly cited.

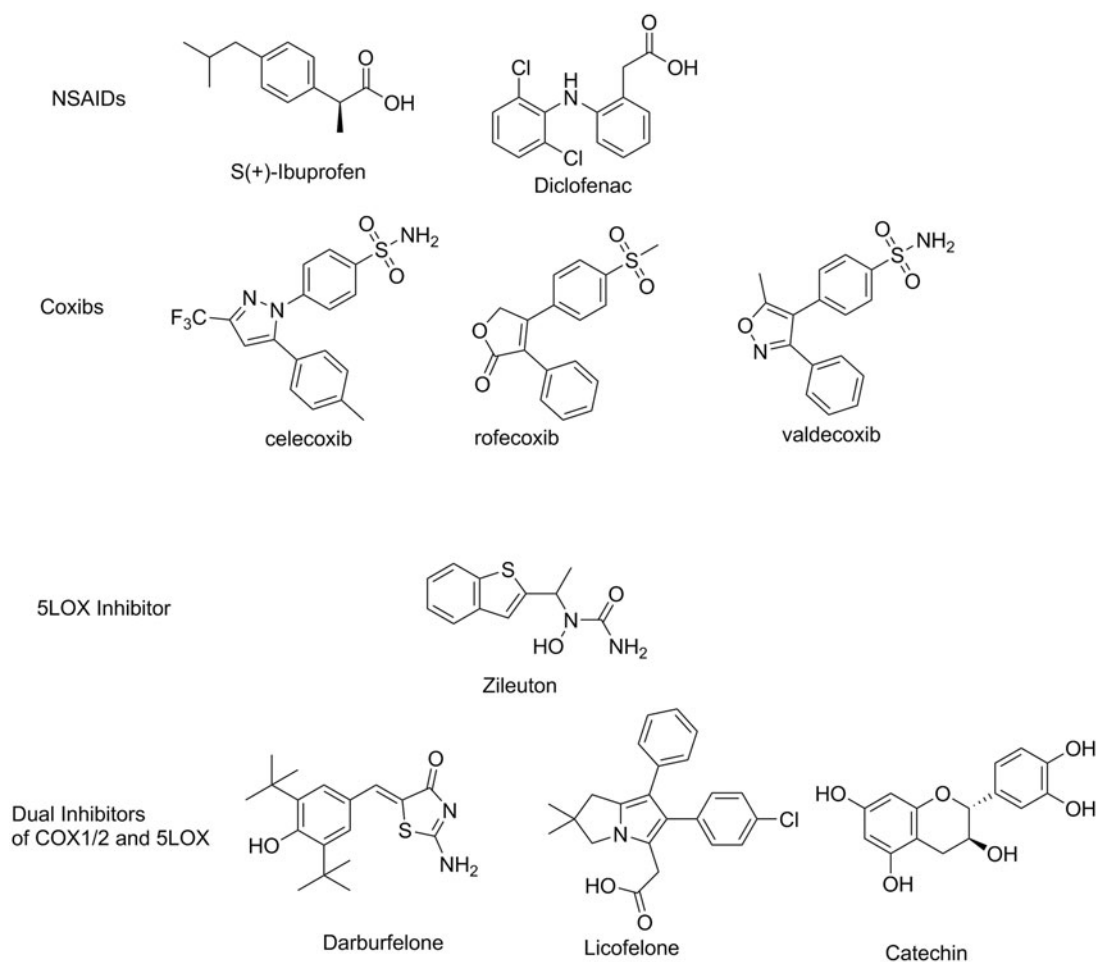


Figure 1. Structures of reported inhibitors of arachidonic acid biosynthesis.

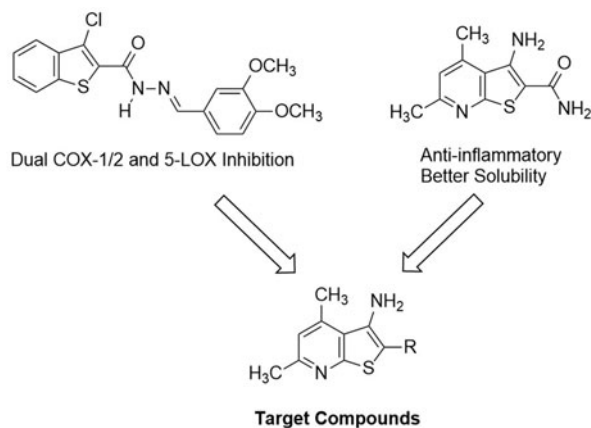


Figure 2. Approach to develop target compounds with dual COX1/2 and 5-LOX inhibition from previously reported compounds.

In addition, dual inhibition of COX1/2 and 5-LOX provided cardio-protective activity in a noteworthy contrast to COX-2 inhibitors²⁴. Efforts for developing clinically useful dual COX1/2–5LOX inhibitors are still active area in drug discovery, since no approval has been granted yet for the first drug in this class². Licofelone, the first clinically studied dual inhibitor has completed phase III clinical trials but it is not clear why it is not marketed yet². The potential benefits of dual COX1/2–5LOX inhibitors extend beyond OA. For instance, they demonstrated anticonvulsant²⁵ as well as anticancer activities^{26,27}.

In our quest to finding novel anti-inflammatory agents, we relied on a screening model which primarily started with measuring the *in vivo* anti-inflammatory activities^{28–30}. On the other hand, we sought 3-aminothieno[2,3-*b*]pyridine as promising molecular entities to develop novel anti-inflammatory agents with possible dual inhibitory mechanism against COX1/2 and 5-LOX. This heterobicyclic scaffold has been studied for its versatile activities against inflammatory disorders, albeit for other subcellular targets^{31–33}. Thienopyridine derivatives have also been reported for their potent anti-proliferative activities^{34,35}. Moreover, our target thieno[2,3-*b*]pyridine is a close congener to benzothiophene, a nucleus recently tested for inhibition of COX1/2 and 5-LOX³⁶ (Figure 2).

Experimental

Chemistry

General methods

All melting points were uncorrected and measured using Electro-thermal IA 9100 apparatus (Shimadzu, Japan); IR spectra were recorded as potassium bromide pellets on a Perkin-Elmer 1650 spectrophotometer (USA), Faculty of Science, Cairo University, Cairo, Egypt. ¹H-NMR spectra were determined on a Varian Mercury (500 MHz) spectrometer (Varian UK) and chemical shifts were expressed as ppm against TMS as an internal reference (Faculty of Science, Cairo University, Cairo, Egypt). Mass spectra were recorded on 70 eV (EI Ms-QP 1000 EX, Shimadzu, Japan),

Faculty of Science, Cairo University, Cairo, Egypt. Microanalyses were operated using Vario, Elementar apparatus (Shimadzu, Japan), Organic Microanalysis Unit, Faculty of Science, Cairo University, Cairo, Egypt. Column Chromatography was performed on (Merck) Silica gel 60 (particle size 0.06–0.20 mm).

Synthesis

1,2-Dihydro-4,6-dimethyl-2-thioxopyridine-3-carbonitrile (1). A mixture of 4,6-dimethyl-3-cyano-2-chloropyridine (1.66 g, 0.01 mol) and thiourea (1.52 g, 0.02 mol) was refluxed in dry ethanol (20 ml) for 6 h³⁷. Then evaporated under reduced pressure and the residue was recrystallised from methanol to give **1**. Yield 68%, m.p. 183 °C (Lit. m.p. 180 °C²⁴).

General procedure for preparation of compounds (2a–c). A mixture of the pyridinethione **1** (1.64 g, 0.01 mol), chloroacetic acid (2.8 g, 0.03 mol), appropriate aldehyde (0.05 mol), and fused sodium acetate (2.0 g) in acetic acid/acetic anhydride (30 ml, 1:1) was heated under reflux for 8 h and left to cool. The solid formed was filtered off and washed with water and recrystallised from ethanol/H₂O to afford **2a–c**.

(±) **3-Benzylidene-3, 8a-dihydro-5,7-dimethyl-2-oxo-2H-thiazolo[3,2-a]pyridine-8-carbonitrile (2a).** Yield: 77%; m.p.: 105–107 °C; IR (KBr) ν (cm⁻¹): 1725 (C=O), 2256 (C≡N). MS (EI) m/z : 294 [M⁺] (85%). ¹H NMR (DMSO-d₆, 500 MHz) δ (ppm): 2.41 (s, 3H, CH₃), 2.75 (s, 3H, CH₃), 5.4 (s, 1H, CH), 6.5 (s, 1H, pyr-H), 6.9 (s, H, =CH), 7.1–7.6 (m, 5H, Ar-H); Anal. Calcd. for C₁₇H₁₄N₂OS (294.08): C, 69.36; H, 4.79; N, 9.52%. Found: C, 69.67; H, 4.42; N, 9.79%.

(±) **3-Furan-2-ylmethylene-3,8a-dihydro-5,7-dimethyl-2-oxo-2H-thiazolo[3,2-a]pyridine-8-carbonitrile (2b).** Yield: 69%; m.p.: 100–102 °C; IR (KBr) ν (cm⁻¹): 1730 (C=O), 2220 (C≡N). MS (EI) m/z : 284 [M⁺] (85%). ¹H NMR (DMSO-d₆, 500 MHz) δ (ppm): 2.12 (s, 3H, CH₃), 2.3 (s, 3H, CH₃), 5.5 (s, 1H, CH), 6.4 (s, 1H, pyr-H), 7.0 (s, H, =CH), 7.1–7.4 (m, 3H, Ar-H); Anal. Calcd. for C₁₅H₁₂N₂O₂S (284.06): C, 63.36; H, 4.25; N, 9.85%. Found: C, 63.14; H, 4.59; N, 9.61%.

(±) **3-(3-Phenyl-allylidene)-3,8a-dihydro-5,7-dimethyl-2-oxo-2H-thiazolo[3,2-a]pyridine-8-carbonitrile (2c).** Yield: 76%; m.p.: 80–82 °C; IR (KBr) ν (cm⁻¹): 1580 (C=C), 1750 (C=O), 2260 (C≡N). MS (EI) m/z : 320 [M⁺] (85%). ¹H NMR (DMSO-d₆, 500 MHz) δ (ppm): 2.2 (s, 3H, CH₃), 2.4 (s, 3H, CH₃), 5.4 (s, 1H, CH), 6.2 (s, 1H, pyr-H), 6.5 (s, H, =CH), 6.7 (s, H, =CH), 7.1 (s, H, =CH), 7.3–7.6 (m, 5H, Ar-H). Anal. Calcd. for C₁₉H₁₆N₂OS (320.1): C, 71.22; H, 5.03; N, 8.74%. Found: C, 71.53; H, 5.28; N, 8.45%.

General procedure for preparation of compounds 3a–b. To an ethanolic sodium hydroxide solution [sodium hydroxide (0.01 mol) in ethanol (20 ml)] pyridinethione **1** (1.64 g, 0.01 mol) was added, with stirring for 30 min, and then the appropriate alkyl halide (0.02 mol) was added drop-wise with vigorous shaking. The reaction mixture was stirred for 2 h at r.t., poured onto cold water (100 ml) and neutralised with dilute HCl. The solid precipitate was filtered off and washed with water and recrystallised from methanol to afford **3a–b**. The reported compound **3b** was prepared in 70% yield and m.p. 93 °C (Lit. m.p. 90 °C)³⁷.

S-Methyl-4, 6-dimethyl-2-thiopyridine-3-carbonitrile (3a). Yield: 72%; m.p.: 80–82 °C; IR (KBr) ν (cm⁻¹): 2218 (C≡N). MS (EI) m/z : 178 [M⁺] (91%). ¹H NMR (DMSO-d₆, 500 MHz) δ (ppm): 2.59 (s, 3H,

CH₃), 2.65 (s, 3H, CH₃), 3.96 (s, 3H, S-CH₃), 6.9 (s, 1H, pyr-H). Anal. Calcd. for C₉H₁₀N₂S (178.25): C, 60.64; H, 5.65; N, 15.72%. Found: C, 60.41; H, 5.84; N, 15.96%.

General procedure for preparation of compounds 4a–c. An excess of aqueous 37% formaldehyde (5–6 ml) was added to a suspension of pyridinethione **1** (1.64 g, 0.01 mol) in EtOH (15 ml). The mixture was heated with stirring to complete dissolution and then the appropriate primary amine (0.01 mol) was added in one portion. The resulting mixture was refluxed with vigorous stirring for 3 min and then stirred at 20 °C for 4 h. The precipitate formed was filtered off and crystallised from ethanol to afford **4a–c**.

(±) **3-Aryl-2,3,4,9a-tetrahydro-6,8-dimethylpyrido[2,1-b][1,3,5]thiadiazine-9-carbonitrile (4a).** Yield: 53%; m.p.: 180–182 °C; IR (KBr) ν (cm⁻¹): 2230 (C≡N). MS (EI) m/z : 283 [M⁺] (69%). ¹H NMR (DMSO-d₆, 500 MHz) δ (ppm): 2.30 (s, 3H, CH₃), 2.58 (s, 3H, CH₃), 4.5 (s, 2H, S-CH₂), 4.9 (s, 2H, N-CH₂), 5.2 (s, 1H, CH), 6.8 (s, 1H, pyr-H), 6.9–7.5 (m, 5H, Ar-H). Anal. Calcd. for C₁₆H₁₇N₃S (283): C, 67.81; H, 6.05; N, 14.83%. Found: C, 67.65; H, 6.31; N, 14.62%.

(±) **3-Aryl-2,3,4,9a-tetrahydro-6,8-dimethylpyrido[2,1-b][1,3,5]thiadiazine-9-carbonitrile (4b).** Yield: 68%; m.p.: 115–117 °C; IR (KBr) ν (cm⁻¹): 2235 (C≡N). MS (EI) m/z : 297 [M⁺] (79%). ¹H NMR (DMSO-d₆, 500 MHz) δ (ppm): 2.1 (s, 3H, CH₃), 2.3 (s, 3H, CH₃), 2.8 (s, 3H, CH₃), 4.6 (s, 2H, S-CH₂), 4.8 (s, 2H, N-CH₂), 5.1 (s, 1H, CH), 6.2 (s, 1H, pyr-H), 7.0–7.5 (m, 4H, Ar-H). Anal. Calcd. for C₁₇H₁₉N₃S (297): C, 68.65; H, 6.44; N, 14.13%. Found: C, 68.31; H, 6.25; N, 14.39%.

(±) **3-Aryl-2,3,4,9a-tetrahydro-6,8-dimethylpyrido[2,1-b][1,3,5]thiadiazine-9-carbonitrile (4c).** Yield: 59%; m.p.: 125–127 °C; IR (KBr) ν (cm⁻¹): 2210 (C≡N). MS (EI) m/z : 297 [M⁺] (72%). ¹H NMR (DMSO-d₆, 500 MHz) δ (ppm): 2.30 (s, 3H, CH₃), 2.58 (s, 3H, CH₃), 4.5 (s, 2H, S-CH₂), 4.7 (s, 2H, CH₂), 5.2 (s, 2H, N-CH₂), 5.9 (s, 1H, CH), 6.8 (s, 1H, pyr-H), 7.2–7.6 (m, 5H, Ar-H). Anal. Calcd. for C₁₇H₁₉N₃S (297): C, 68.65; H, 6.44; N, 14.13%. Found: C, 68.88; H, 6.71; N, 14.00%.

Ethyl-3-amino-4,6-dimethylthieno[2,3-b]pyridine-2-carboxylate (5). This compound was prepared by two methods.

Method 1: A mixture of pyridinethione **1** (1.64 g, 0.01 mol) and ethyl bromoacetate (3.34 g, 0.02 mol) in dry ethanol (50 ml) containing sodium metal (1 g) was stirred for 2 h, and then was refluxed with stirring for 4 h. The reaction mixture was cooled and poured into ice water. The solid formed was filtered off, dried, and recrystallised from methanol to afford **5**.

Method 2: A mixture of ethyl 2-(3-cyano-4,6-dimethylpyridin-2-ylthio)acetate **3b** (2.5 g, 0.01 mol) and dry ethanol (50 ml) containing sodium ethoxide (2%) was refluxed with stirring for 4 h. The reaction mixture was cooled and poured into ice water. The solid formed was filtered off, dried, and recrystallised from ethanol to afford **5**.

Yield 70%, m.p. 138 °C (Lit. m.p. 135 °C²⁴).

3-Amino-4,6-dimethylthieno[2,3-b]pyridine-2-carbazide (6). A mixture of thienopyridine-2-carboxylate **5** (2.5 g, 0.01 mol) and hydrazine hydrate (0.05 mol, 99%) in absolute ethanol (15 ml) was heated under reflux for 6 h. The reaction mixture was concentrated, cooled, and the precipitate formed was filtered and crystallised from ethanol to afford **6**. Yield 70%, m.p. 200 °C (Lit. m.p. 198 °C)³⁷.

General procedure for preparation of compounds 7a–c. A mixture of thienopyridine-2-carbazide (2.36 g, 0.01 mol) and the appropriate aldehyde (0.02 mol) in pyridine:ethanol (15:20 ml) was heated

under reflux for 2 h. The reaction mixture was cooled and poured into ice water. The solid formed was filtered off, dried, and crystallised from the acetic acid to afford **7a-c**.

3-Amino-4,6-dimethyl-thieno [2,3-b] pyridine-2-carboxylic acid benzylidene-hyrazide (7a). Yield: 65%; m.p.: 250–252 °C; IR (KBr) ν (cm^{-1}): 3100, 3260, 3310 (NH)(NH₂), 1690 (C=O), 1230 (C=N). MS (EI) m/z : 324 [M^+] (76%). ¹H NMR (DMSO-*d*₆, 500 MHz) δ (ppm): 2.32 (s, 3H, CH₃), 2.71 (s, 3H, CH₃), 7.0 (s, 1H, pyr-H), 6.9 (s, 2H, NH₂, D₂O exchangeable), 7.3–7.6 (dd, 5H, Ar-H), 8.2 (s, 1H, NH, D₂O exchangeable), 8.5 (s, 1H, CH). Anal. Calcd. for C₁₇H₁₆N₄OS (324): C, 62.94; H, 4.97; N, 17.27%. Found: C, 62.97; H, 4.62; N, 17.62%.

3-Amino-4,6-dimethyl-thieno [2,3-b] pyridine-2-carboxylic acid (4-chloro-benzylidene)-hyrazide (7b). Yield: 72%; m.p.: 280–282 °C; IR (KBr) ν (cm^{-1}): 3150, 3290, 3310 (NH)(NH₂), 1685 (C=O), 1245 (C=N). MS (EI) m/z : 358 [M^+] ³⁵Cl (66%), 360 [$\text{M} + 2$] ³⁷Cl (22%). ¹H NMR (DMSO-*d*₆, 500 MHz) δ (ppm): 2.45 (s, 3H, CH₃), 2.62 (s, 3H, CH₃), 6.9 (s, 1H, pyr-H), 7.0 (s, 2H, NH₂, D₂O exchangeable), 7.2–7.5 (dd, 4H, Ar-H), 8.3 (s, 1H, NH, D₂O exchangeable), 8.6 (s, 1H, CH). Anal. Calcd. for C₁₇H₁₅ClN₄OS (358): C, 56.90; H, 4.21; N, 15.61%. Found: C, 56.46; H, 4.49; N, 15.93%.

3-Amino-4, 6-dimethyl-thieno [2,3-b] pyridine-2-carboxylic acid (4-methoxy-benzylidene)-hyrazide (7c). Yield: 74%; m.p.: 270–272 °C; IR (KBr) ν (cm^{-1}): 3180, 3240, 3320 (NH)(NH₂), 1680 (C=O), 1220 (C=N), 1150 (C–O). MS (EI) m/z : 354 [M^+] (58%). ¹H NMR (DMSO-*d*₆, 500 MHz) δ (ppm): 2.32 (s, 3H, CH₃), 2.61 (s, 3H, CH₃), 3.5 (s, 3H, CH₃), 6.8 (s, 1H, pyr-H), 7.0 (s, 2H, NH₂, D₂O exchangeable), 7.2–7.6 (dd, 4H, Ar-H), 8.0 (s, 1H, NH, D₂O exchangeable), 8.6 (s, 1H, CH). Anal. Calcd. for C₁₈H₁₈N₄O₂S (354): C, 61.00; H, 5.12; N, 15.81%. Found: C, 61.33; H, 5.45; N, 15.56%.

General procedure for preparation of compounds 8a–c. To an ice-cooled solution of the corresponding thienopyridine-2-carboxylic acid arylidine-hydrazide **7a–c** (0.01 mol) in AcOH (20 ml) and conc. HCl (3 ml) a cold solution of sodium nitrite (0.23 g in 5 ml of water) was added drop-wise over 5 min. The solution was stirred at room temperature for 3 h at 0–5 °C; where a solid was formed, collected by filtration, dried, and crystallised from dioxane to afford **8a–c**.

7,9-Dimethyl-3-[(phenylmethylene)amino]pyrido[3',2':4,5]-thieno[3,2-d][1,2,3]triazin-4(3H)-one (8a). Yield: 72%; m.p.: 300–302 °C; IR (KBr) ν (cm^{-1}): 1690 (C=O), 1250 (C=N). MS (EI) m/z : 335 [M^+] (45%), ¹H NMR (DMSO-*d*₆, 500 MHz) δ (ppm): 2.35 (s, 3H, CH₃), 2.75 (s, 3H, CH₃), 6.8 (s, 1H, pyr-H), 7.3–7.6 (m, 5H, Ar-H), 8.2 (s, 1H, CH). Anal. Calcd. for C₁₇H₁₃N₅OS (335): C, 60.88; H, 3.91; N, 20.88%. Found: C, 60.47; H, 3.64; N, 20.57%.

7,9-Dimethyl-3-[(4-chloro-phenyl-methylene)amino]pyrido[3',2':4,5]thieno [3,2-d][1,2,3]triazin-4(3H)-one (8b). Yield: 74%; m.p.: 255–257 °C; IR (KBr) ν (cm^{-1}): 1685 (C=O), 1270 (C=N). MS (EI) m/z : 369 [M^+] ³⁵Cl (60%), 371 [$\text{M} + 2$] ³⁷Cl (20%). ¹H NMR (DMSO-*d*₆, 500 MHz) δ (ppm): 2.45 (s, 3H, CH₃), 2.62 (s, 3H, CH₃), 6.9 (s, 1H, pyr-H), 7.2–7.5 (dd, 4H, Ar-H), 8.3 (s, 1H, CH). Anal. Calcd. for C₁₇H₁₂ClN₅OS (369): C, 55.21; H, 3.27; N, 18.94%. Found: C, 55.49; H, 3.51; N, 18.72%.

7,9-Dimethyl-3-[(4-methoxy-phenyl-methylene)amino]pyrido[3',2':4,5]thieno [3,2-d][1,2,3]triazin-4(3H)-one (8c). Yield: 65%; m.p.: 240–242 °C; IR (KBr) ν (cm^{-1}): 1680 (C=O), 1240 (C=N), 1150

(C–O). MS (EI) m/z : 365 [M^+] (56%), ¹H NMR (DMSO-*d*₆, 500 MHz) δ (ppm): 2.32 (s, 3H, CH₃), 2.61 (s, 3H, CH₃), 3.5 (s, 3H, CH₃), 7.0 (s, 1H, pyr-H), 7.2–7.6 (dd, 4H, Ar-H), 8.6 (s, 1H, CH). Anal. Calcd. for C₁₈H₁₅N₅O₂S (365): C, 59.16; H, 4.14; N, 19.17%. Found: C, 59.42; H, 4.41; N, 19.54%.

General procedure for preparation of compounds 9a–b. A mixture of thienopyridine-2-carbazide **6** (2.36 g, 0.01 mol) and ethyl acetoacetate (1.3 g, 0.01 mol) or acetylacetone (1 g, 0.01 mol) in glycolic acetic acid (30 ml) was heated under reflux for 5 h. The excess solvent was evaporated under reduced pressure to one-third of the solution and the reaction mixture was allowed to cool. The precipitate formed was collected and crystallised from the acetic acid to afford **9a** and **9b**.

3-Amino-2-[carbonyl (3-methyl-4,5-dihydro-5H-pyrazol-5-on-1-yl)]-4,6-dimethylthieno [2,3-b] pyridine (9a). Yield: 59%; m.p.: 140–142 °C; IR (KBr) ν (cm^{-1}): 3425, 3265 (NH₂), 1686 (C=O). MS (EI) m/z : 302 [M^+] (71%), ¹H NMR (DMSO-*d*₆, 500 MHz) δ (ppm): 2.00 (s, 3H, CH₃), 2.29 (s, 3H, CH₃), 2.65 (s, 3H, CH₃), 2.9 (s, 2H, CH₂), 5.58 (s, 2H, NH₂, D₂O exchangeable), 6.9 (s, 1H, pyr-H).; Anal. Calcd. for C₁₄H₁₄N₄O₂S (302.35): C, 55.61; H, 4.67; N, 18.53%. Found: C, 55.39; H, 4.90; N, 18.81%.

3-Amino-2-[carbonyl (3,5-dimethyl-pyrazol-1-yl)]-4,6-dimethylthieno[2,3-b] pyridine (9b). Yield: 67%; m.p.: 150–152 °C; IR (KBr) ν (cm^{-1}): 3425, 3265 (NH₂), 1686 (C=O). MS (EI) m/z : 300 [M^+] (62%), ¹H NMR (DMSO-*d*₆, 500 MHz) δ (ppm): 2.38 (s, 3H, CH₃), 2.65 (s, 3H, CH₃), 2.79 (s, 6H, two CH₃), 5.2 (s, 2H, NH₂, D₂O exchangeable), 7.1 (s, 1H, pyr-H), 8.2 (s, 1H, 4H-pyrazole). Anal. Calcd. for C₁₅H₁₆N₄OS (300.38): C, 59.98; H, 5.37; N, 18.65%. Found: C, 59.68; H, 5.68; N, 18.40%.

General procedure for preparation of compounds 10a–b. A mixture of thienopyridine-2-carbazide **6** (0.01 mol) in formic acid (15 ml) or acetic anhydride (15 ml) was heated under reflux for 6 h. The excess solvent was evaporated *in vacuo* (to one-third of the solution) and cooled; the solid was collected by filtration, dried, and crystallised from acetic acid to afford **10a–b**.

7,9-Dimethyl-3-fomylaminopyrido [3',2':4,5]thieno[3,2-d]pyrimidin-4(3H)-one (10a). Yield: 48%; m.p.: 220–222 °C; IR (KBr) ν (cm^{-1}): 1715, 1760 (two C=O). MS (EI) m/z : 274 [M^+] (71%), ¹H NMR (DMSO-*d*₆, 500 MHz) δ (ppm): 2.4 (s, 3H, CH₃), 2.8 (s, 3H, CH₃), 7.1 (s, 1H, pyr-H), 7.9 (s, 1H, CH pyrimidine), 8.5 (s, 1H, H-C=O), 9.5 (s, 1H, NH). Anal. Calcd. for C₁₂H₁₀N₄O₂S (274.3): C, 52.54; H, 3.67; N, 20.43%. Found: C, 52.81; H, 3.41; N, 20.69%.

3-Diacetyl-amino-2,7,9-trimethylpyrido [3',2':4,5]thieno[3,2-d]pyrimidin-4(3H)-one (10b). Yield: 65%; m.p.: 133–135 °C; IR (KBr) ν (cm^{-1}): 1720, 1745, 1780 (three C=O). MS (EI) m/z : 344 [M^+] (65%), ¹H NMR (DMSO-*d*₆, 500 MHz) δ (ppm): 1.9 (s, 3H, CH₃), 2.2 (s, 3H, CH₃), 2.5 (s, 3H, CH₃), 2.7 (s, 6H, 2CH₃), 7.2 (s, 1H, pyr-H). Anal. Calcd. for C₁₆H₁₆N₄O₃S (344.09): C, 55.80; H, 4.68; N, 16.27%. Found: C, 56.00; H, 4.91; N, 16.50%.

Biological assay

Animals

To define the minimum total sample size and the average number for each group the *a priori* test with the following parameters was

conducted: anticipated effect size (Cohen's *d*): 0.7; desired statistical power level: 0.8; probability level: 0.05. The *a priori* test calculation returned the following values: minimum total sample size (one-tailed hypothesis)³⁸; minimum sample size per group (one-tailed hypothesis)³⁹.

According to *a priori* test results, experiments were conducted on young adult male Sprague–Dawley rats (5 rats per group), weighing 140–170 g. The animals were housed at cages in a temperature controlled ($25 \pm 1^\circ\text{C}$) environment and were fed *ad libitum* with standard laboratory chow and allowed free access to water. This investigation conforms to the ethical Guide for the Care and Use of Laboratory Animals published by the US National Institutes of Health (NIH Publication No. 85–23, revised in 1996). The animal protocol is in accordance with the Animal Ethical Care regulations in the Faculty of Pharmacy, Helwan University.

Assessment of anti-inflammatory activity

Compounds (equimolar to the reference drug) were dissolved in DMSO and administrated subcutaneously. One hour later, paw oedema was induced by subplantar injection of 0.1 ml of 1% carrageenan (Sigma-Aldrich, St. Louis, MO) into the right hind paw. Paw volume was measured using a water plethysmometer (Basile, Comerio, Italy). The difference between the right and left paw volume was measured at 1, 2, 3, and 4 h after induction of inflammation.

The control group (five rats per group) received DMSO subcutaneously and carrageenan in the subplantar region. Results were expressed as percentage inhibition of inflammation. Ibuprofen (70 mg kg^{-1}) was used as the reference drug⁴⁰.

Biochemical assay

Drugs capacities to inhibit COX-1, COX-2, and 5-LOX enzymes were assessed using ELISA kits; COX-1 (human) Inhibitor Screening Assay Kit (Item № 701070), COX-2 (human) Inhibitor Screening Assay Kit (Item № 701080), and 5-LOX Inhibitor Screening Assay Kit (Item № 760700) from Cayman (Ann Arbor, MI). The used protocol was according to the manufacturer protocol guide and instructions using ELISA plate reader.

Statistics. All assays results are expressed as mean \pm standard error of the mean (SEM). The comparisons between the control and the treatment groups were carried out using One-way ANOVA using a statistical package (SPSS version 17.0). A *p* value of <0.05 was considered significant.

Molecular modelling

All molecular modelling work was performed using SYBYL-X package (www.certara.com) installed with licence to the Faculty of Pharmacy, King Abdulaziz University on Windows 7-operated computer, equipped with Samsung SyncMaster 2233RZ 120 Hz LCD DisplayTM (3D ready) and Nvidia Geforce 3D Vision Glasses KitTM.

Preparation of protein and ligands

Crystal structures were downloaded as .pdb files from Protein Databank Website (www.rcsb.org). The initial biopolymers were simplified by deleting all but one monomer in the quaternary structures and then prepared for docking. The previous two steps were performed using “Biopolymer” Tools.

The Ligand Structures Library was built on Chemschetch⁴¹ and saved as .sd files. The structures were converted to 3D and optimised using SYBYL-X's Concord embedded in “Prepare Ligands” tools.

Surflex docking

Docking was performed using Surflex programme embedded in “Dock Ligand” tools. First, the target previously prepared protein was selected and underwent final preparation for docking. Surflex docking was performed after protomol generation on ligand mode.

Manual docking

Ligand preparation. The manual docking was used in case no ligand was present to guide Surflex automatic docking procedure. This protocol was used only for docking experiments of syn-**7a**, anti-**7a**, and **8c** to the active site of 5-LOX crystal structure (PDB Code 3O8Y) because it contains no ligand to guide a Surflex automatic docking. In this regards, ligands prepared above we further optimised to the global minimum conformation by energy minimisation tools until the global minimum is reached (Termination: Gradient).

Docking. We used three-step, visually-guided procedure (Place-Merge-MD) as follows.

1. *Place.* Prepared protein structure (as described above) and the intended ligand were imported to two different SYBYL-X screen levels. The ligand was moved until it was visually entered the active site. Careful inspection of features in the ligand and residues around to ensure maximum positive interactions with the least clashes with the active site residues.

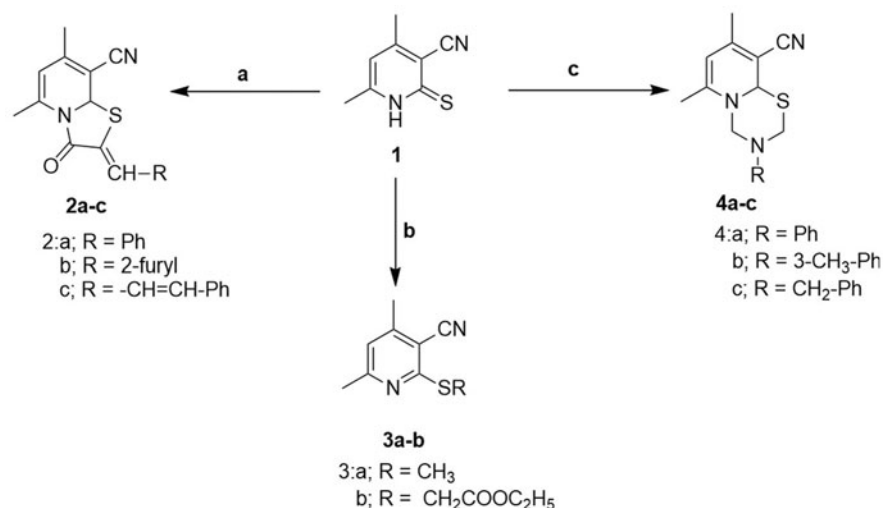
2. *Merge.* When convinced that the ligand is situated in the best docking position, the ligand was merged into the protein screen. To confirm that the ligand has no serious clash with the active site residues, AAs with 5 Å sphere distance around the docked ligand were unhidden. If a clash existed, another round of moving the ligand was performed and the procedure is repeated until the least possible clash is reached. After merge, the energy of the complex is measured and compared to uncomplexed protein. The process is repeated several times with different docking modes. The best docking complexes pose according to visual inspection of clashes and energy computation were retained and compared. The poses ranked according to their energies (first priority) and positive interactions of the ligand with the active site.

3. *Molecular dynamics (MD).* Molecular dynamics was performed to check the stability of the complex generated by manual docking according to the following protocol with time length 1000 fs at 300 K and 0 atm pressure. Snapshots every 5 fs were taken and inspected visually. The best snapshot in energy is considered provided that a minimum movement of the protein loops are observed.

Results

Chemical synthesis

Thienopyridine synthesis has been previously reported⁴². Synthesis of target anti-inflammatory compounds was accomplished *via* the



Scheme 1. Utilisation of compound **1** to produce series **2–4** (a = ClCH₂COOH, Ac₂O, AcOH, NaOAc along with an aldehyde RCHO, b = RX where X = Br or I, c = RNH₂ and HCHO).

key intermediate pyridin-2-thione (compound **1**), which was prepared according to the reported method³⁷. Compound **1** was then utilised in different reactions to yield three different series of compounds^{2–4}. Condensation of **1** with chloroacetic acid and certain aldehydes in a mixture of acetic acid and acetic anhydride gave the thiazolopyridine derivatives **2a–c**⁴³. Compound **1** was also treated with different alkylating agents to afford the corresponding 2-alkylthio analogues **3a–b**. Condensation of **1** with formalin or certain primary amines afforded the pyridothiadiazine derivatives **4a–c** (Scheme 1).

Compound **3b** was subsequently converted to the thienopyridine derivatives **5** via reaction with NaOEt/EtOH. Compound **5** was treated with NH₂NH₂ to yield the corresponding hydrazide **6** (Scheme 2)³⁷.

The intermediate compound **6** was used as a diversity precursor to prepare a number of target compounds' series^{7–11}. Compound **6** was reacted with certain aldehydes to give the corresponding arylidene hydrazide **7a–c** which were subsequently reacted with NaNO₂/HCl to afford the pyrido[3',2':4,5]thieno[3,2-d][1,2,3]triazin-4(3H)-one **8a–c**⁴⁴. In addition, condensation of compound **6**, with ethyl acetoacetate, acetylacetone or carbon disulphide to afford the derivatives **9a–c** respectively. Finally, the reaction of **6**, separately with HCOOH and acetic anhydride afforded the pyridothienodiazine analogues **10a** and **10b**, respectively (Scheme 3).

Biological screening

In vivo anti-inflammatory assay

The obtained compounds were tested for their anti-inflammatory activity using the carrageenan-induced rat paw oedema assay. Compound potency and duration of action were compared with those of the reference compound ibuprofen. The *in vivo* anti-inflammatory activity is shown in Figure 3.

Compounds **7a**, **7b**, **8b**, and **8c** induced a satisfactory anti-inflammatory activity, exceeding that of ibuprofen at the 4 h time interval. The compounds produced 73.5, 73.2, 78.2, and 79.4% inhibition respectively, compared to 69.5% inhibition for ibuprofen. The time–activity profiles of these compounds are commensurate to that of ibuprofen, varying only in the onset of action. Compounds of series **7** showed a more rapid onset than

ibuprofen, while those of series **8** showed a much slower onset (Supplementary Table S1).

In vitro inhibition assays of 5LOX, COX-2, COX-1 enzymes

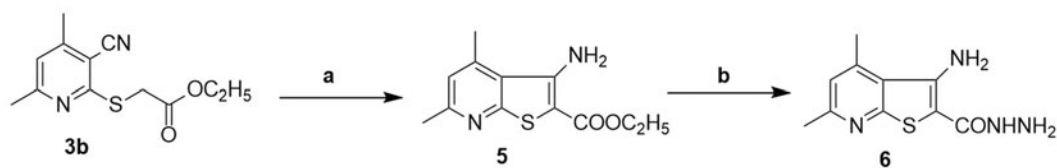
The compounds belonging to series **7** and **8** were subjected to enzyme assay investigations against 5-LOX, COX-1, and COX-2. Those compounds were chosen based on the demonstrated profound anti-inflammatory activity in the above *in vivo* test.

Discussion

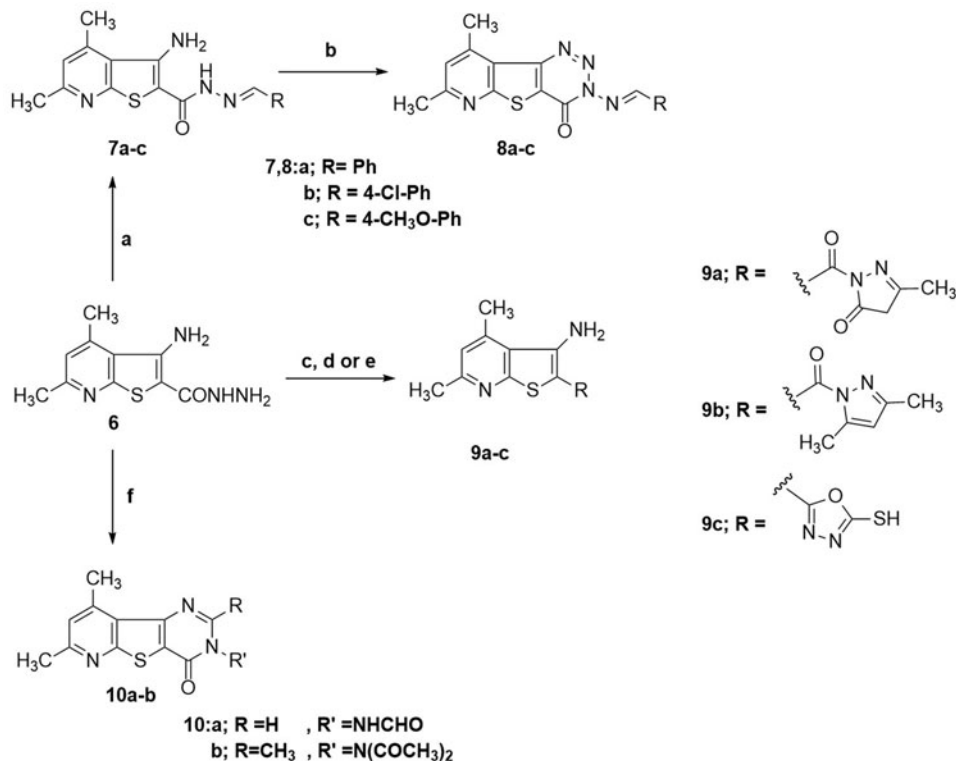
The phenotypic screening preceding isolated enzyme assays provided an opportunity to shift focus towards series of compounds that exhibited higher potential therapeutic benefit. The structure–activity relationship (SAR) of screened compounds for *in vivo* anti-inflammatory activities favoured thieno[2,3-*b*]pyridines over other scaffolds such as **2** and **4**. The 5-LOX inhibition assay, however, favoured the hydrazides **7** as the most potent compound, **7a**, is 35 and 87 times higher than the tricyclic derivatives **8a** and **8c**, respectively. A similar result was noticed in the COX-2 inhibition assay, albeit to a lower extent. In this regard, **7a** inhibited COX-2 at 3.6 and 1.8 times higher than **8a** and **8c**, respectively.

Results, displayed in Table 1, were interesting since potency level, as well as selectivity between the two series **7** and **8**, explained the potential of these compounds. The *in vitro* enzyme inhibition assays revealed that compounds **7a** and **7b** realised higher potency and selectivity towards 5-LOX and COX-2 over COX-1. They are also higher than the compounds **8b** and **8c** as well as ibuprofen⁴⁵ in their 5-LOX and COX-2 inhibition potency. Compounds **7a** and **7b** are also more selective than the other three compounds towards COX-2 than COX-1 with selectivity index COX-2/COX-1 = 4.6 and 4.2 for **7a** and **7b**, respectively. Compound **8b** and **8c** demonstrated approximately 2-fold more affinity towards COX-1 over COX-2.

The lack of proportionality between *in vitro* and *in vivo* read-outs can be attributed to several common factors, mainly pharmacokinetic parameters (absorption, distribution, metabolism, and excretion) that account for discriminations in drug efficacies⁴⁶.



Scheme 2. Conversion of **3b** to thienopyridine derivatives (a = NaOEt/EtOH, b = NH₂NH₂).



Scheme 3. Various reactions of compound **6** to afford the target compound series **7-10** (a = RCHO, b = NaNO₂, HCl, c = ethyl acetoacetate, d = acetylacetone, e = CS₂, f = HCOOH or Ac₂O).

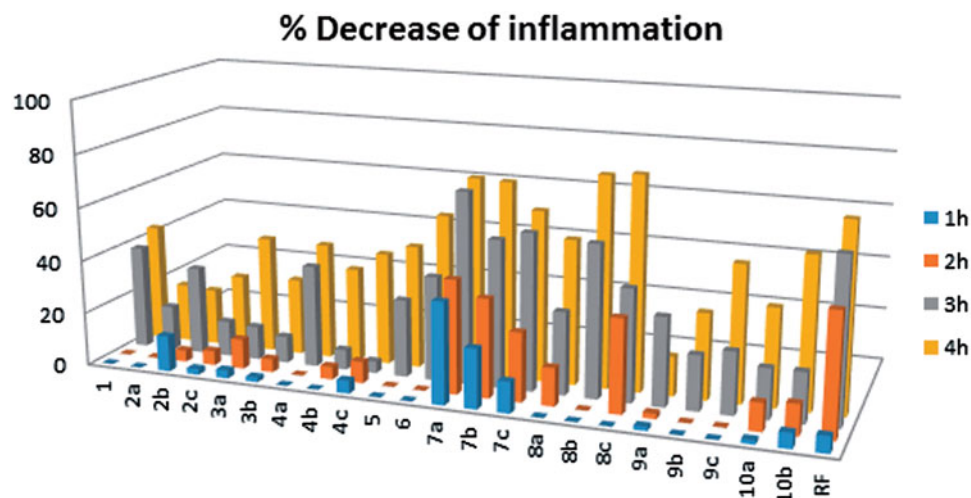


Figure 3. *In vivo* anti-inflammatory assay of thieno[2,3-*b*]pyridine derivatives. The anti-inflammatory potency is proportional to the height of the bar (inhibition %). The height of the bars (inhibition%) = (swell.drug/swell.control)100. Swell = mean difference in rat paw volume between right and left paw. RF = ibuprofen (reference drug). For more details, refer [Supplementary Table S1](#).

A structure-based analysis by docking selected compounds in the active site of 5-LOX, COX-2, and COX-1 was conducted to propose an understanding of the enzyme inhibition assay results. Crystal structures from the Protein Databank website (www.rcsb.org)

were downloaded and employed in the study, accession codes: 3O8Y for 5-LOX⁴⁷, 4PH9 for COX-2⁴⁸ and 1EQG for COX-1³⁸. All the molecular modelling work was carried out using SYBLYL-X v.2.1 package licenced to King Abdulaziz University according to

Table 1. Enzyme inhibition assay results for COX-1, COX-2, and 5-LOX along with per cent inflammation reduction at the 4 h time interval in the rat paw oedema assay.

Compound	5-LOX IC ₅₀ (μM)	COX-2 IC ₅₀ (μM)	COX-1 IC ₅₀ (μM)	inflammation reduction % (4h)
7a	0.154	9.988	45.869	73.54
7b	0.279	7.524	31.797	73.02
8b	13.520	35.990	19.902	78.23
8c	5.419	18.992	7.663	79.36
Ibuprofen	0.436	43.628	31.945	69.52

All standard error of means (SEM) are lower than 10%.

methodologies and protocols described in the “Experimental” section and detailed in [Supplementary Material](#).

Among all crystal structures of 5-LOX, only three entries belong to *H. sapiens* 5-LOX (Entries: 3O8Y, 3V98, and 3V99). All of these crystal structures are mutated by replacing three lysines (K⁶⁵³KK⁶³⁵) into Glutamic acid–Asparagine–Leucine (ENL). The latter two entries had additional mutation S663D which resulted in the loss of 5-LOX activity (converted to 15-LOX-like activity)⁴⁹. Therefore, we settled with 3O8Y as our target for docking experiments.

The active site of 5-LOX is framed by two α -helices, the α 2-helix and the arched helix, forming an elongated U-shaped hydrophobic cavity that accommodates the substrate AA, a 20-carbon polyunsaturated fatty acid⁵⁰. There is a catalytic iron nearby the active site but access to this iron is regulated by the side chains of Phe-177 and Tyr-181 (the FY cork), which also caps the cavity once the substrate enters the active site⁴⁷. The defined conformation of this active site helped in understanding the clearly higher 5-LOX inhibitory activities of **7a** and **7b** (IC₅₀ are at nanomolar level) over the cyclised analogues **8b** and **8c** (IC₅₀ are at micromolar level).

To rationalise the higher activity of **7a** and **7b** against 5-LOX, a study of different **7a** conformers was carried out. The *anti*-conformer is the calculated global minimum and it was found to be 3.8 kcal/mol less energy than the *syn*-conformer. This *anti*-conformer can make an intramolecular hydrogen bonding between the 3-amino and the carbonyl oxygen, more efficiently than that of the *syn*-conformer ([Supplementary Material](#)). It is therefore proposed that the *anti*-conformer of **7a** attains a higher population.

Interestingly, the pyrido[3',2':4,5]thieno[3,2-d][1,2,3]triazin-4(3H)-one derivatives⁸ attain a global minimum conformation that well overlaps with the *syn*-conformation of **7a**. For docking experiments into 5-LOX crystal structure, we used visually guided manual docking followed by molecular dynamics (MD), since the active site contained no ligand to guide the automatic docking process by Surflex⁵¹. All three conformers (*anti*-**7a**, *syn*-**7a** and **8c**) could rest inside the active site of the human 5-LOX in a hydrophobic tunnel between the α 2 helix and the arched helix considering the least steric clashes with surrounding residues ([Figure 4](#)). Moreover, according to the proposed model, our compounds established several hydrophobic contacts within convenient van der Waals distances with hydrophobic residues lining the active site. The *anti*-conformer of the most active compound **7a** made attractions with side chains of Leu-373, Leu-368, Ile-406, Leu-414, and Leu-607. In addition, *anti*-**7a** is theorised to form a crucial hydrogen bonding interaction through the hydrazide NH to Asn-407, an important residue of the arched helix that contributes to the shape of the active site. Surprisingly, the pyridine nitrogen of within the thieno[2,3-*b*]pyridine nucleus formed what is possibly a very important ionic interaction with Glu-376 side chain carboxylate with all three docked structures (*anti*-, *syn*-**7a** as well as **8a**).

Compound **8b** was approximately 90 times less potent than **7a** in inhibiting 5-LOX in enzyme inhibition assays. This can be explained using the structure-based analysis of an affinity model with 5-LOX active site. As mentioned above, both **8b** and **8c** resemble the *syn*-conformation of **7a**. These entities were

generally able to maintain the major polar and non-polar interactions with the active site residues. However, **8b** approached Ile-415 and Leu-368 side chains inconveniently, thus making possible clashes with the active site in this docking mode ([Supplementary Material](#)). To be accommodated in the active site, significant shifts in the primary backbone protein loops have to be made after the MD step. Therefore, it should be challenging to predict the actual binding mode of this compound in this less flexible closed active site.

According to this model, it is noted that the 4,6-dimethylthieno[2,3-*b*]pyridine scaffold has a good physicochemical balance in the molecular properties as it rests in a dominantly lipophilic pocket. The two methyl groups bolstered the aromatic ring hydrophobic attractions with Leu-368 and Leu-373 side chains (residues of α 2 helix, [Figure 4](#)) while the pyridine nucleus conferred a much needed polar character to our compounds.

Lead compounds' affinity towards COX-2 were investigated in a virtual screening model using Surflex docking application embedded in SYBYL-X package and the Surflex docking scores were compared⁵¹. For this purpose, we initially chose a crystal structure of COX-2 containing ibuprofen (Code: 4PH9), the reference drug for both *in vivo* and *in vitro* screenings. Our analysis suggests possible binding modes of the tricyclic analogue **8c** reasonably. The active site of COX-2 is composed of four main regions according to the crystal structures; the main hydrophobic channel, the polar mouth area (mainly side chains of Arg-120 and Tyr-355), the selectivity side pocket and another smaller hydrophobic pocket near the mouth area⁵². Therefore, in a previous model, we reported that a pyridylurea derivative of naproxen binds possibly by inserting the naphthalene moiety properly deep in the main channel. Meanwhile, the urea group makes several hydrogen bonding with the polar area near the active site mouth²⁸. In our present work, compound **8c** was predicted to insert the bulky thieno[2,3-*b*]pyridine moiety into the hydrophobic channel and make hydrophobic contacts with side chains of Val-344, Tyr-348, Val-349, Phe-385, Trp-387, Leu-531, and Leu-534 ([Figure 5](#)). The triazine ring and imine group form a network of hydrogen bonding with the guanidine side chains of Arg-120 and the phenol group of Tyr-355 (similar to ibuprofen's carboxylate interactions). The terminal aryl group of Schiff base was directed to the outside of the protein surface possibly because this tricyclic ligand does not enjoy much flexibility.

A limitation of this model is that it was not successful in describing the good binding of **7a**, from our perspective. The top-scoring pose ([Table 2](#)) of this bicyclic compound, being more flexible than **8c**, was placed by Surflex as a *syn*-conformer while directing its thieno[2,3-*b*]pyridine moiety towards the hydrophobic channel. It also forced the terminal phenyl group of the Schiff base to an *eclipsed* torsion that penetrated the characteristic side pocket of COX-2. We had some concerns about this suggested model of **7a** because it was predicted to be half the potency of **8c** according to Surflex scores ([Table 2](#)). In addition, the docking conformation, though filled the side pocket, did not make any significant polar interactions (*cf.* **8c**) with the active site polar region.

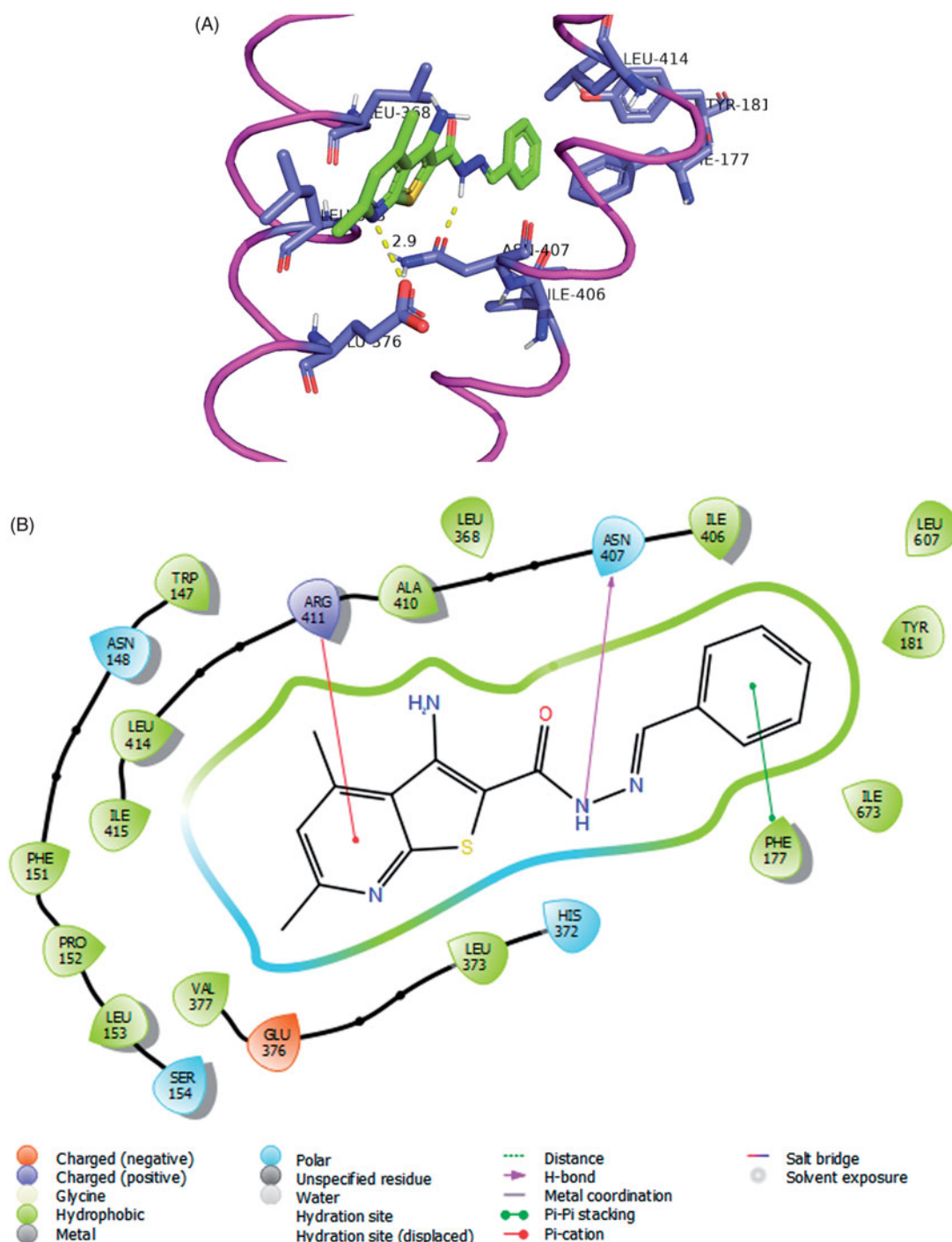


Figure 4. (A) Compound **7a** (coloured green) docked into the active site of 5-LOX. The $\alpha 2$ helix is seen to the left and the arched helix is located to the right (both coloured magenta). The hydrophobic residues interacting with the ligand Leu-368, Leu-373 (of $\alpha 2$ helix), Ile-406, and Leu-414 (of arched helix) are shown. The FY cork residues Phe-177 and Tyr-181 are seen to the top of the image. The graphics of this image was generated using Pymol free software (<https://pymol.org/2/>). (B) 2D representation of the interactions of **7a** with the active site of 5-LOX generated using Maestro visualiser.

This limitation highlights that this model is merely a speculative trial to explain the enzyme inhibition activities of the reported compounds.

We suspected that the protomol formation did not help the model prediction efficiency because the process is known to be affected by the co-crystallised ligand's size and shape⁵¹. In addition, the main channel of the active site of this crystal structure is seemingly shrunk tightly around the small isobutyl tail of ibuprofen, the co-crystallised ligand. Therefore, we decided to perform the modelling work on another COX-2 crystal structure (PDB Code:

3OLU) that contained arachidonic acid glyceryl ester as a co-crystallised ligand of larger size⁵³. The larger ligand gave rise to a significantly longer but narrower protomol in the main channel pocket (Supplementary Material). The docking experiments of the four compounds to the active site returned different predictions of binding modes (Figure 6(B)). The Schiff base group was inserted inside the main hydrophobic channel (reverse mode to the previous model on 4PH9). Both ligands (**7a** and **8c**) made hydrogen bonding with Ser-530 side chain. It is worthy to mention that Ser-530 is a residue involved in the catalytic peroxidation of AA

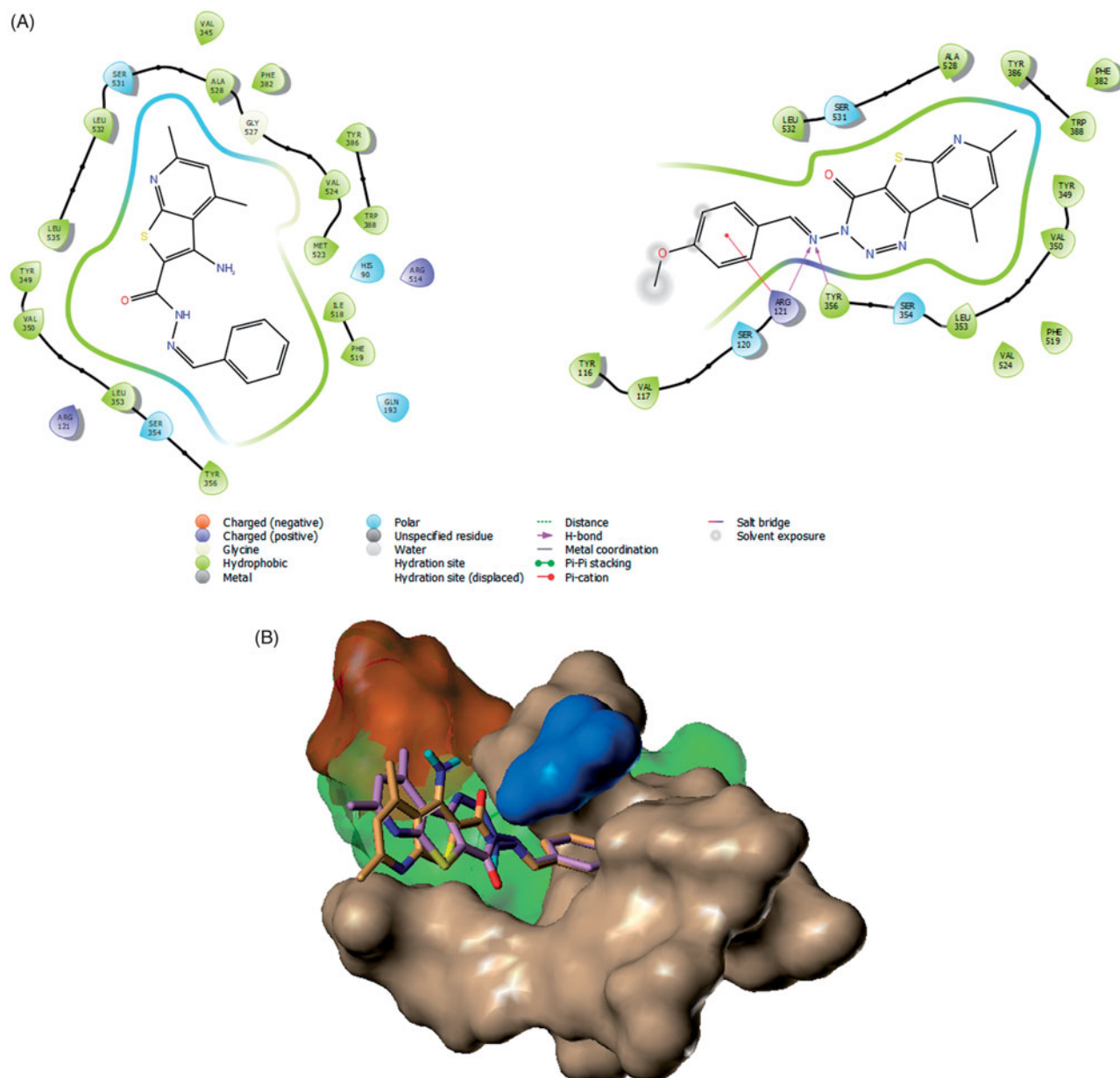


Figure 5. Docking of **7a** and **8b** to COX-2 crystal structures. (A) 2D representation of the binding modes of compounds **7a** (left) and compound **8c** (right) with the active site of COX-2 generated using Maestro visualiser. (B) Model of docking of **7a** (violet) and **8c** (Orange) on COX-2 crystal structure (Code: 3OLU). The active site pocket is coloured green as determined by Surflex's protomol except the side pocket, which was given an orange surface. Surface of the active site's main hydrophobic channel residues are coloured coffee-brown. Ser-530 is given a blue surface.

Table 2. Surflex total scores of docked compounds into COX-2 (Code 4PH9 and 3OLU) and COX-1 (1EQG).

Compound	Surflex docking score		
	4PH9	3OLU	1EQG
lbu	7.5	6.8	6.5
8d	7.7	7.2	4.6
8b	5.7	6.3	3.9
7a	4.0	5.7	1.3
7b	2.3	6.2	1.2

Surflex docking score = Calculated $-\log K_d$

substrate, forming a hydrogen bond with the carboxylic group of diclofenac, and being acetylated by acetylsalicylic acid as proven by structural biology reports⁵⁴. Compound **7a** in this model existed in the previously predicted more probable *anti*-

conformation (~ 17 kcal/mol lower than that of the first docking model). The bulkier thieno[2,3-*b*]pyridine moiety was oriented towards the outside of the active site with shallow penetration of the selectivity pocket. Based on these assumptions, the model also helped explain the slight selectivity of **7a** to COX-2 over COX-1 (Will be discussed later in further details). In our analysis, this model had improved predictions but it is not free from concerns. The much lipophilic dimethyl pyridyl ends are projecting outside the active site to the aqueous medium. In addition, the impact of the substituents on the Schiff base phenyl groups on the experimental activities are not supported by this model. Finally, the calculated scores in this model still rank **8b** and **8c** higher than **7a** and **7b** but the differences in the total Surflex scores are not as drastic as the first model (for the 4PH9 structure) (Table 2). Since the experimental differences between the ligands are not drastic either, the model might be considered qualitatively aligned with

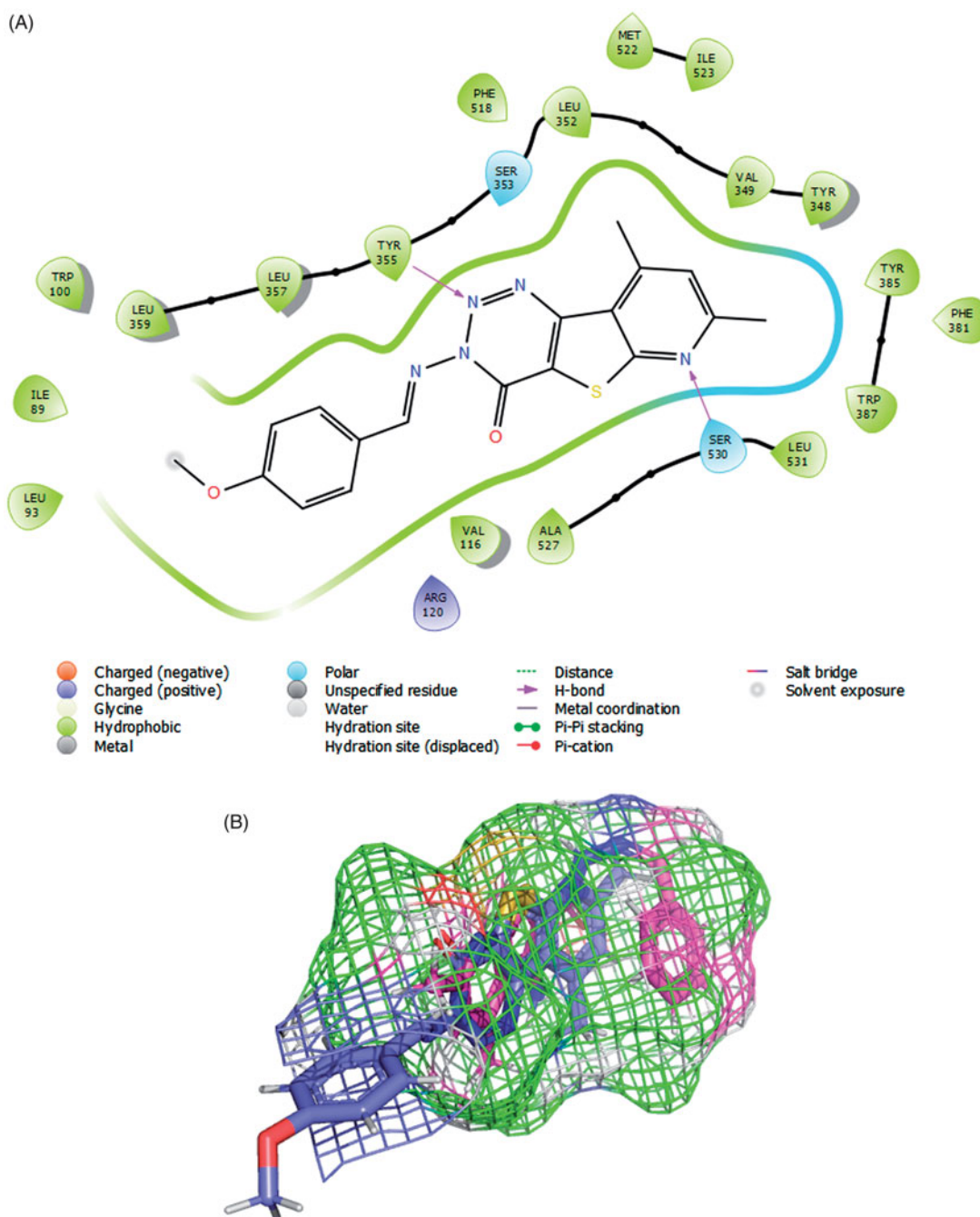


Figure 6. (A) **8c** (violet) and **7a** (magenta) in COX-1 active site as determined by Surflex Graphics of this image was generated using Pymol free software (<https://pymol.org/2/>). (B) 2D diagram showing the putative model of binding mode of compound **8c** with COX-1 active site (PDB Code: 1EQG).

the experimental results to provide a possible explanation of the relative compounds' activities. We expect that the scoring, as well as the binding modes, may vary if we use different crystal structure entries among the many available in the PDB website.

Modelling the COX-1 inhibition was performed on a crystal structure that also contained ibuprofen as a ligand (PDB Code: 1EQG)³⁸. It is established that there are several common features between COX-1 and COX-2 active sites, the main hydrophobic channel, the catalytic Ser-530 and the mouth having polar residues such as Arg-120. However, COX-1 is characterised by the absence of the side pocket and by a narrower main hydrophobic channel⁵⁵. In docking experiments, Surflex successfully granted **8c** the highest scoring on COX-1, which aligns with experimental results (Tables 1 and 2). The dimethyl pyridine moiety reached the

hydrophobic bottom of the main channel and was adjusted to form a hydrogen bond with Ser-530. The terminal triazine ring formed a bifurcate hydrogen bonding with Tyr-355. The rigid nature of **8c** added convincing evidence for a high probability of its postulated binding mode. Meanwhile, Surflex placed the flexible Schiff base end of **7a** to the bottom of the active site and twisted the imine side chain to fill this pocket. This way, the *anti*-conformer of the ligand was totally immersed inside the active site assuring that the dimethylpyridyl end is exposed to a hydrophobic microenvironment. No effective polar contacts were observed for the ligand (Figure 6). We checked if the linear global energy minimum would give a better binding quality by a manual docking experiment but found serious steric clash with Val-518 (Supplementary Material).

In conclusion, this modelling work provided a hypothetical rationale of speculative binding modes of the title compounds and improved our understanding of the experimental results because it reasonably aligned these calculations with experimental results within a plausible margin of deviation.

Acknowledgment

Authors thank the Faculty of Pharmacy, King Abdulaziz University for permission to use their SYBYL-X molecular modeling package in this research.

Disclosure statement

Authors declare no conflict of interest in this work with any potentially affected party by results of this study. The authors also declare no influence of any second party on designing of conducting the study.

Funding

This work was partially supported by two grants from Helwan University. M. E. E. received a grant for purchasing chemicals. The second grant was given to the Department of Pharmaceutical Organic Chemistry for spectroscopic and elemental analyses. The authors are thankful to Helwan University for financial support.

References

- Dennis EA, Norris PC. Eicosanoid storm in infection and inflammation. *Nat Rev Immunol* 2015;15:511–23.
- Elliott JA, Smith HS. Handbook of acute pain management. Boca Raton (FL): CRC Press; 2016.
- Funk CD. Prostaglandins and leukotrienes: advances in eicosanoid biology. *Science* 2001;294:1871–5.
- Harizi H, Corcuff J-B, Gualde N. Arachidonic-acid-derived eicosanoids: roles in biology and immunopathology. *Trends Mol Med* 2008;14:461–9.
- Smith WL, Urade Y, Jakobsson P-J. Enzymes of the cyclooxygenase pathways of prostanoid biosynthesis. *Chem Rev* 2011;111:5821–65.
- FitzGerald GA, Patrono C. The coxibs, selective inhibitors of cyclooxygenase-2. *N Engl J Med* 2001;345:433–42.
- Melnikova I. Future of COX2 inhibitors. *Nat Rev Drug Discov* 2005;4:453–4.
- Khanna D, Khanna PP, Furst DE. COX-2 controversy: where are we and where do we go from here? *Inflammopharmacology* 2005;13:395–402.
- Bello AE, Holt RJ. Cardiovascular risk with non-steroidal anti-inflammatory drugs: clinical implications. *Drug Saf* 2014;37:897–902.
- Scifinder (Scifinder.cas.org) for “COX-1 Housekeeping” returned 161 references that used this term to date (6 Dec 2017).
- Prochazkova M, Dolezal T, Sliva J, Krsiak M. Different Patterns of Spinal cyclooxygenase-1 and cyclooxygenase-2 mRNA expression in inflammatory and postoperative pain. *Basic Clin Pharmacol Toxicol* 2006;99:173–7.
- Wallace JL, Chapman K, McKnight W. Limited anti-inflammatory efficacy of cyclo-oxygenase-2 inhibition in carrageenan-airpouch inflammation. *Br J Pharmacol* 1999;126:1200–4.
- Martinez-Gonzalez J, Badimon L. Mechanisms underlying the cardiovascular effects of COX-inhibition: benefits and risks. *Curr Pharm Des* 2007;13:2215–27.
- Suleyman H, Demircan B, Karagoz Y. Anti-inflammatory and side effects of cyclooxygenase inhibitors. *Pharmacol Rep* 2007;59:247.
- Marcouiller P, Pelletier J-P, Guévremont M, et al. Leukotriene and prostaglandin synthesis pathways in osteoarthritic synovial membranes: regulating factors for interleukin 1 β synthesis. *J Rheumatol* 2005;32:704–12.
- Rainsford K. Leukotrienes in the pathogenesis of NSAID-induced gastric and intestinal mucosal damage. *Inflamm Res* 1993;39:C24–26.
- Funk CD. Role of leukotrienes revealed by targeted disruption of the 5-lipoxygenase gene. *Nature* 1994;372:10.
- Luo M, Lee S, Brock T. Leukotriene synthesis by epithelial cells. *Histol Histopathol* 2003;18:587–95.
- Bouchette D, Pellegrini MV, Zileuton. StatPearls [Internet]. Treasure Island (FL): StatPearls Publishing; 2018.
- Weinblatt M, Kremer J, Coblyn J, et al. Zileuton, a 5-lipoxygenase inhibitor in rheumatoid arthritis. *J Rheumatol* 1992;19:1537–41.
- Samuelsson B, Dahlen S-E, Lindgren JA, et al. Leukotrienes and lipoxins: structures, biosynthesis, and biological effects. *Science* 1987;237:1171–6.
- Wittenberg RH, Willburger RE, Kleemeyer KS, Peskar BA. In vitro release of prostaglandins and leukotrienes from synovial tissue, cartilage, and bone in degenerative joint diseases. *Arthritis Rheumatol* 1993;36:1444–50.
- Sharma RN, Xavier FP, Vasu KK, et al. Synthesis of 4-benzyl-1,3-thiazole derivatives as potential anti-inflammatory agents: an analogue-based drug design approach. *J Enzyme Inhibit Med Chem* 2009;24:890–7.
- Martel-Pelletier J, Lajeunesse D, Reboul P, Pelletier JP. Therapeutic role of dual inhibitors of 5-LOX and COX, selective and non-selective non-steroidal anti-inflammatory drugs. *Ann Rheum Dis* 2003;62:501–9.
- Deshmukh R, Goyal A, Sharma P. Licofelone: A dual COX/5-LOX inhibitor attenuates intracerebroventricular streptozotocin-induced cognitive deficit, oxidative stress and neuro-inflammatory cytokines in rats. *Alzheimer's Dement* 2013;9:P302.
- Sharma B, Paliania P, Singh P. Modeling of cyclooxygenase-2 and 5-lipoxygenase inhibitory activity of apoptosis-inducing agents potentially useful in prostate cancer chemotherapy: derivatives of diarylpyrazole. *J Enzyme Inhibit Med Chem* 2009;24:607–15.
- Kumar G, Patlolla JMR, Madka V, et al. Simultaneous targeting of 5-LOX-COX and ODC block NNK-induced lung adenoma progression to adenocarcinoma in A/J mice. *Am J Cancer Res* 2016;6:894.
- Ammar YA, Fayed EA, Bayoumi AH, et al. Design and synthesis of pyridine-amide based compounds appended naproxen moiety as anti-microbial and anti-inflammatory agents. *Am J PharmTech Res* 2015;5:245–73.
- Abouzid KA, Khalil NA, Ahmed EM, et al. Structure-based molecular design, synthesis, and in vivo anti-inflammatory activity of pyridazinone derivatives as nonclassic COX-2 inhibitors. *Med Chem Res* 2010;19:629–42.
- El-Araby M, Omar A, Hassanein HH, et al. Design, synthesis and in vivo anti-inflammatory activities of 2,4-diaryl-5-4H-imidazolone derivatives. *Molecules* 2012;17:12262–75.
- Zeng X-X, Zheng R-L, Zhou T, et al. Novel thienopyridine derivatives as specific anti-hepatocellular carcinoma (HCC)

- agents: synthesis, preliminary structure–activity relationships, and in vitro biological evaluation. *Bioorg Med Chem Lett* 2010;20:6282–5.
32. Morwick T, Berry A, Brickwood J, et al. Evolution of the thienopyridine class of inhibitors of IkappaB kinase-beta: part I: hit-to-lead strategies. *J Med Chem* 2006;49:2898–908.
 33. Liu H, Li Y, Wang X-Y, et al. Synthesis, preliminary structure–activity relationships, and in vitro biological evaluation of 6-aryl-3-amino-thieno [2, 3-b] pyridine derivatives as potential anti-inflammatory agents. *Bioorg Med Chem Lett* 2013;23:2349–52.
 34. Zafar A, Pilkington LI, Haverkate NA, et al. Investigation into improving the aqueous solubility of the thieno[2,3-b]pyridine anti-proliferative agents. *Molecules* 2018;23:E145.
 35. Zafar A, Sari S, Leung E, et al. GPCR modulation of thieno[2,3-b]pyridine anti-proliferative agents. *Molecules* 2017;22:E2254.
 36. El-Miligy MM, Hazzaa AA, El-Messmary H, et al. New benzo-thiophene derivatives as dual COX-1/2 and 5-LOX inhibitors: synthesis, biological evaluation and docking study. *Future Med Chem* 2017;9:443–68.
 37. Yassin F. Synthesis, reactions and biological activity of 2-substituted 3-cyano-4, 6-dimethylpyridine derivatives. *Chem Heterocyclic Comp* 2009;45:35–41.
 38. Selinsky BS, Gupta K, Sharkey CT, Loll PJ. Structural analysis of NSAID binding by prostaglandin H2 synthase: time-dependent and time-independent inhibitors elicit identical enzyme conformations. *Biochemistry* 2001;40:5172–80.
 39. El-Sayed M-IK, Amin HA-KA. Mechanism of endothelial cytoprotective and thrombo-resistance effects of sildenafil, vardenafil and tadalafil in male rabbit. *Arch Med Sci* 2015;11:190.
 40. Wisniewski-Rebecca ES, Rocha BA, Wiirzler LA, et al. Synergistic effects of anethole and ibuprofen in acute inflammatory response. *Chem Biol Interact.* 2015;242:247–53.
 41. ACD/Labs, ChemSketch version 12.01, Advanced Chemistry Development, Inc., Toronto, On, Canada, www.acdlabs.com, 2015.
 42. Pilkington LI, Haverkate NA, Van Rensburg M, et al. Synthesis of 3-Amino-2-carboxamide tetrahydropyrrolo [2, 3-b] quinolines. *Synlett* 2016;27:2811–4.
 43. Khalifa NM, Abdel-Rahman AA, El Gwaad AAA, Al-Omar MA. Synthesis and characterization of some novel substituted thiazolo [3, 2-a] pyridine and thioxopyrimido [4, 5-d] pyrimidine derivatives. *Asian J Chem* 2014;26:8202.
 44. Elneairy MA, Gad-Elkareem MA, Abdel-Fattah AM. Thieno [2, 3-b] pyridine-2-carbohydrazide in polyheterocyclic synthesis: the synthesis of pyrido [3', 2': 4, 5] thieno [3, 2-d] pyrimidine, pyrido [3', 2': 4, 5] thieno [3, 2-d][1, 2, 3] triazine, and pyrazolyl, oxadiazolylthieno [2, 3-b] pyridine derivatives. *Phosphorus Sulfur Silicon* 2006;181:1451–66.
 45. Rainsford KD. Ibuprofen: a critical bibliographic review. Boca Raton (FL): CRC Press; 2003.
 46. Borchardt R, Kerns E, Hageman M, et al. Optimizing the “drug-like” properties of leads in drug discovery. Berlin: Springer; 2007.
 47. Gilbert NC, Bartlett SG, Waight MT, et al. The structure of human 5-lipoxygenase. *Science* 2011;331:217–9.
 48. Orlando BJ, Lucido MJ, Malkowski MG. The structure of ibuprofen bound to cyclooxygenase-2. *J Struct Biol* 2015;189:62–6.
 49. Gilbert NC, Rui Z, Neau DB, et al. Conversion of human 5-lipoxygenase to a 15-lipoxygenase by a point mutation to mimic phosphorylation at Serine-663. *FASEB J* 2012;26:3222–9.
 50. Neau DB, Gilbert NC, Bartlett SG, et al. The 1.85 Å structure of an 8R-lipoxygenase suggests a general model for lipoxygenase product specificity. *Biochemistry* 2009;48:7906–15.
 51. Jain AN. Surflex: fully automatic flexible molecular docking using a molecular similarity-based search engine. *J Med Chem* 2003;46:499–511.
 52. Kurumbail RG, Stevens AM, Gierse JK, et al. Structural basis for selective inhibition of cyclooxygenase-2 by anti-inflammatory agents. *Nature* 1996;384:644–8.
 53. Vecchio AJ, Malkowski MG. The structural basis of endocannabinoid oxygenation by cyclooxygenase-2. *J Biol Chem* 2011;286:20736–45.
 54. Kalgutkar AS, Crews BC, Rowlinson SW, et al. Aspirin-like molecules that covalently inactivate cyclooxygenase-2. *Science* 1998;280:1268–70.
 55. Luong C, Miller A, Barnett J, et al. Flexibility of the NSAID binding site in the structure of human cyclooxygenase-2. *Nat Struct Biol* 1996;3:927–33.